Dark matter and collider signals in supersymmetric $U(1)'$ models with nonuniversal Z' couplings

Mariana Frank[*]

Department of Physics, Concordia University, 7141 Sherbrooke Street West, Montreal, Québec H4B 1R6, Canada

Katri Huitu[†] and Subhadeep Mondal[‡]

Department of Physics, and Helsinki Institute of Physics, University of Helsinki, P.O. Box 64, Helsinki FI-00014, Finland

(Received 25 September 2019; published 9 December 2019)

We analyze supersymmetric models augmented by an extra $U(1)$ gauge group. To avoid anomalies in these models without introducing exotics, we allow for family-dependent $U(1)'$ charges, and choose a simple form for these, dependent on one $U(1)'$ charge parameter only. With this choice, Z' decays into ditaus but not dileptons, weakening considerably the constraints on its mass. In the supersymmetric sector, the effect is to lower the singlino mass, allowing it to be the dark matter candidate. We investigate the dark matter constraints and collider implications of such models, with mostly singlinos, mostly Higgsinos, or a mixture of the two as the lightest supersymmetric particles. In these scenarios, Z' decays significantly into chargino or neutralino pairs, and thus indirectly into final state leptons. We devise benchmarks which, with adequate cuts, can yield signals visible at the high-luminosity LHC.

DOI: 10.1103/PhysRevD.100.115018

I. INTRODUCTION

Models with additional $U(1)$ gauge are a popular extension of the Standard Model (SM). Without supersymmetry, it was shown that they can provide a model for dark matter [1–4], better agreement with measurements of the anomalous magnetic moment of the muon [5,6], and explain leptogenesis [7]. In supersymmetry, they are motivated by the ability to generate the μ parameter at the electroweak scale [8–13]. If the extra $U(1)'$ is a result of breaking of $E6$, right-handed neutrinos emerging from the 27 fundamental representation can be incorporated into the model spectrum [14]. An added benefit of supersymmetric models is that these explain the stability of the proton [15], and provide fermion masses through the Froggatt-Nielsen mechanism [16].

Extra $U(1)$ symmetries [which we shall refer to as $U(1)'$ models] can arise as low-energy manifestations of grand unified theories [17], of string theories [18], and from models with dynamical electroweak breaking [19]. In the framework of gauge mediation, they provide a mechanism for supersymmetry breaking [20]. A disadvantage of these models is the requirement of cancellation of anomalies. One usually requires to add several exotics to the spectrum [21] in order to make the theory anomaly free. Thus several new particles are introduced with respect to the minimal content, which often spoils the gauge coupling unification,[1] a desirable prediction of the minimal supersymmetric standard model (MSSM) with weak scale soft masses.

The goal of this work is to explore the consequences of an anomaly-free $U(1)'$ model without additional exotic matter, without imposing that it be generated by the breaking of $SO(10)$ or $E6$. We also want to construct a model where we can relax the mass constraints on Z'. Constructing anomaly-free $U(1)'$ models without exotics is possible, but it involves allowing flavor nonuniversality, that is, allowing fermions to have family-dependent $U(1)'$ charges [23]. These charges must be chosen such that all anomaly coefficients cancel, including those from mixed anomalies involving $U(1)'$ charges, and gauge-gravity anomalies. These particular theories have received more

[*]mariana.frank@concordia.ca
[†]katri.huitu@helsinki.fi
[‡]subhadeep.mondal@helsinki.fi

[1]Note however that coupling unification can sometimes be preserved, as in [22], where, in the $U(1)'_N$ model, resulting from breaking supersymmetric $E6$, gauge unification is preserved, even in the presence of exotic remnants of $SU(5)$ representations.

attention lately, given the LHCb measurements of lepton flavor nonuniversality in B-meson decays [24–26].

There are numerous possibilities for nonuniversal $U(1)'$ charges. These are classified in [27] and various aspects of their phenomenological implications have been studied both within non-SUSY and SUSY frameworks [28–34]. In this work, we revisit the supersymmetric $U(1)'$ models with nonuniversal charges, opting for a simple family-dependent choice. Our aim is to study the phenomenology of the Z' boson, which in these scenarios can be light.[2] In addition to consequences observable at colliders, the Z' mass plays a role in fine-tuning, rendering scenarios with a low Z' mass interesting theoretically. We explore how restrictive the Z' mass is, and the signatures of such a boson at the colliders.

Related to these, we also investigate the phenomenology of dark matter in these models [38–41], with an emphasis on the effects of a lighter Z', and on the possibility of having the singlino [the fermion partner of the singlet Higgs boson required to break $U(1)'$ symmetry] as a nonstandard dominant component of dark matter.

As an artifact of allowing flavor nonuniversality, the Z' phenomenology at the LHC can be quite distinctive. The Z' can now decay into certain favored final states dominantly, while some of the more commonly observable decay modes are absent altogether. Here, one possible solution to the various anomaly-cancellation equations leads to a scenario where the Z' is forbidden to decay into electron or muon pairs. Instead, its single most prominent decay mode is $\tau\bar{\tau}$. Naturally, in this scenario, the existing constraints on the Z' mass can be quite relaxed. On the other hand, within a SUSY framework, there can be additional decay modes of the Z' which may lead to hitherto unexplored signal regions. We have explored two such signal regions and present our results in the context of a high-luminosity run of the LHC at a center-of-mass energy of 14 TeV.

The paper is organized in the following way. In Sec. II we describe briefly the theoretical framework of our study. In Sec. III we discuss the impact of various LHC search results on the parameter space of our model. Based on that study, we proceed to select some representative benchmark points. In Sec. IV we discuss the strategy to explore these classes of benchmark points at the 14 TeV LHC. We discuss possible signal regions, SM background contributions and kinematic cuts that can be used to suppress these background contributions and make the signal observable. We discuss our results through detailed cut-flow tables and finally conclude our observations in Sec. V.

[2]In models with universal $U(1)'$ charges, Z' masses are restricted rather stringently by the ATLAS [35] and CMS [36] collaborations, and expected to be around 4–4.5 TeV. These models can be rendered leptophobic by using kinetic mixing between the two $U(1)$ gauge groups, as in e.g., [37].

TABLE I. The particle content of the $U(1)'$ model, and assignments under the different groups, allowing for different charges under the $U(1)'$ group. The index i runs over three families.

	$SU(3)_c$	$SU(2)_L$	$U(1)_Y$	$U(1)'$
Q_i	**3**	**2**	1/6	Q_{Q_i}
U_i^c	$\bar{\mathbf{3}}$	**1**	−2/3	$Q_{U_i^c}$
D_i^c	$\bar{\mathbf{3}}$	**1**	1/3	$Q_{D_i^c}$
L_i	**1**	**2**	−1/2	Q_{L_i}
E_i^c	**1**	**1**	1	$Q_{E_i^c}$
H_u	**1**	**2**	1/2	Q_{H_u}
H_d	**1**	**2**	−1/2	Q_{H_d}
S	**1**	**1**	0	Q_S

II. THE $U(1)'$ MODEL WITH NONUNIVERSAL CHARGES

Supersymmetric $U(1)'$ models are based on the gauge group $SU(3)_c \otimes SU(2)_L \otimes U(1)_Y \otimes U(1)'$, with gauge couplings g_s, g_2, g_Y and g'.[3] The particle spectrum of the models is that of the MSSM augmented by a gauge singlet S, charged under $U(1)'$ only. The particle content, allowing for nonuniversal charges under the $U(1)'$ group, is given in Table I.

The breaking of the $U(1)'$ gauge symmetry down to electromagnetism is achieved through the neutral components of the scalar Higgs fields acquiring VEVs, $\langle H_u^0\rangle = v_u/\sqrt{2}$, $\langle H_d^0\rangle = v_d/\sqrt{2}$ and $\langle S\rangle = v_S/\sqrt{2}$.

The superpotential takes the form

$$\hat{W} = \lambda \hat{S}\hat{H}_d\hat{H}_u + h_u^{ij}\hat{U}_j^c\hat{Q}_i\hat{H}_u + h_d^{ij}\hat{D}_j^c\hat{Q}_i\hat{H}_d + h_e^{ij}\hat{E}_j^c\hat{L}_i\hat{H}_d. \tag{2.1}$$

Here the first term of the superpotential is responsible for generating an effective μ parameter $\lambda\langle S\rangle$, providing a dynamical solution to the μ problem when $\langle S\rangle \sim \mathcal{O}(\text{TeV})$. The rest of the operators in (2.1) are the usual Yukawa term interactions of leptons and quarks.

The most general holomorphic Lagrangian responsible for soft supersymmetry breaking is

$$\begin{aligned} -\mathcal{L}_{\text{soft}} = &\left(\sum_i M_i\lambda_i\lambda_i - A_\lambda \lambda S H_d H_u - A_u^{ij}h_u^{ij}U_j^c Q_i H_u \right.\\ &\left. - A_d^{ij}h_d^{ij}D_j^c Q_i H_d - A_e^{ij}h_e^{ij}E_j^c L_i H_d + \text{H.c.}\right)\\ &+ m_{H_u}^2|H_u|^2 + m_{H_d}^2|H_d|^2 + m_S^2|S|^2 + m_{Q_{ij}}^2\tilde{Q}_i\tilde{Q}_j^*\\ &+ m_{U_{ij}}^2\tilde{U}_i^c\tilde{U}_j^{c*} + m_{D_{ij}}^2\tilde{D}_i^c\tilde{D}_j^{c*} + m_{L_{ij}}^2\tilde{L}_i\tilde{L}_j^*\\ &+ m_{E_{ij}}^2\tilde{E}_i^c\tilde{E}_j^{c*} + \text{H.c.}, \end{aligned} \tag{2.2}$$

[3]The $SU(2)_L \times U(1)_Y \times U(1)'$ covariant derivative is given by $D_\mu = \partial_\mu + ig_2T^aW_\mu^a + ig_YYV_\mu + ig'Y'V'_\mu$.

where the SUSY-breaking sfermion mass-squared $m^2_{Q,\ldots,E^c}$ and the trilinear couplings $A_{u,\ldots,e}$ are 3×3 matrices in flavor space, and are assumed here to be diagonal, while gaugino masses M_i and trilinear couplings $A_{S,\ldots,e}$ are taken to be real.

Family-dependent $U(1)'$ charge assignment forbids some of the Yukawa couplings in the superpotential, resulting in massless fermions. One therefore must introduce a non-holomorphic SUSY breaking Lagrangian, induced by the couplings of fermions to the "wrong" Higgs doublet,

$$-\mathcal{L}_c = C_E^{ij} H_u^* \tilde{L}^i \tilde{E}_R^{cj} + C_U^{ij} H_d^* \tilde{Q}^i \tilde{U}_R^{cj} + C_D^{ij} H_u^* \tilde{Q}^i \tilde{D}_R^{cj} + \text{c.c.}, \tag{2.3}$$

which is essential for giving mass to fermions. The fermion masses are generated at the one loop level through sfermion-gaugino loops [23].

For the theory to be anomaly free, the $U(1)'$ charges must satisfy conditions requiring vanishing of $U(1)'-SU(3)-SU(3)$, $U(1)'-SU(2)-SU(2)$, $U(1)'-U(1)_Y-U(1)_Y$, $U(1)'$-graviton-graviton, $U(1)'-U(1)'-U(1)_Y$ and $U(1)'-U(1)'-U(1)'$ anomalies, that is, the charges must satisfy, respectively,

$$0 = \sum_i (2Q_{Q_i} + Q_{U_i^c} + Q_{D_i}) \tag{2.4}$$

$$0 = \sum_i (3Q_{Q_i} + Q_{L_i}) + Q_{H_d} + Q_{H_u} \tag{2.5}$$

$$0 = \sum_i \left(\frac{1}{6}Q_{Q_i} + \frac{1}{3}Q_{D_i^c} + \frac{4}{3}Q_{U_i^c} + \frac{1}{2}Q_{L_i} + Q_{E_i^c}\right) + \frac{1}{2}(Q_{H_d} + Q_{H_u}) \tag{2.6}$$

$$0 = \sum_i (6Q_{Q_i} + 3Q_{U_i^c} + 3Q_{D_i^c} + 2Q_{L_i} + Q_{E_i^c}) + 2Q_{H_D} + 2Q_{H_u} + Q_s \tag{2.7}$$

$$0 = \sum_i (Q_{Q_i}^2 + Q_{D_i^c}^2 - 2Q_{U_i^c}^2 - Q_{L_i}^2 + Q_{E_i^c}^2) - Q_{H_d}^2 + Q_{H_u}^2 \tag{2.8}$$

$$0 = \sum_i (6Q_{Q_i}^3 + 3Q_{D_i^c}^3 + 3Q_{U_i^c}^3 + 2Q_{L_i}^3 + Q_{E_i}^3) + 2Q_{H_d}^3 + 2Q_{H_u}^3 + Q_S^3. \tag{2.9}$$

A possible solution to the above, satisfying the anomaly cancellation requirement, is

$$\begin{aligned} &Q_{E_{1,2}} = Q_{L_{1,2}} = Q_{L_3} = 0 \\ &Q_{Q_i} = \frac{Q_{E_3}}{9}; \qquad Q_{D_i} = -\frac{Q_{E_3}}{9}; \qquad Q_{U_i} = -\frac{Q_{E_3}}{9}; \\ &Q_{H_u} = 0; \qquad Q_{H_d} = -Q_{E_3}; \qquad Q_S = Q_{E_3}, \end{aligned} \tag{2.10}$$

which is by no means general, but allows us to express all $U(1)'$ charges in terms of a single one, Q_{E_3}.

A. Neutralino sector

In this framework, the neutralino mass matrix in the basis $(\lambda_U, \lambda_{\tilde{B}}, \tilde{W}, \tilde{H}_d^0, \tilde{H}_u^0, \tilde{S})$ is of the following form:

$$\begin{pmatrix} M_4 & 0 & 0 & g'Q_{H_d}v_d & g'Q_{H_u}v_u & g'Q_S v_S \\ 0 & M_1 & 0 & -\frac{1}{2}g_1 v_d & \frac{1}{2}g_1 v_u & 0 \\ 0 & 0 & M_2 & \frac{1}{2}g_2 v_d & -\frac{1}{2}g_2 v_u & 0 \\ g'Q_{H_d}v_d & -\frac{1}{2}g_1 v_d & \frac{1}{2}g_2 v_d & 0 & -\frac{1}{\sqrt{2}}v_S\lambda & -\frac{1}{\sqrt{2}}v_u\lambda \\ g'Q_{H_u}v_u & \frac{1}{2}g_1 v_u & -\frac{1}{2}g_2 v_u & -\frac{1}{\sqrt{2}}v_S\lambda & 0 & -\frac{1}{\sqrt{2}}v_d\lambda \\ g'Q_S v_S & 0 & 0 & -\frac{1}{\sqrt{2}}v_u\lambda & -\frac{1}{\sqrt{2}}v_d\lambda & 0 \end{pmatrix}. \tag{2.11}$$

It is evident from the neutralino mass matrix that the lightest supersymmetric particle (LSP) can be singlino dominated only if $g'Q_S v_S$ is small enough and M_4 is heavy enough to be decoupled from the singlino mass. When all other soft masses are decoupled and there is almost zero mixing, the singlino mass is simply driven by the parameters g', Q_S and v_S. These parameters also drive the Z' mass and as a result, if one looks for a light Z', a light singlino is always obtained. Depending on the choice of λ, the Higgsinos can be light as well. In our present study, we have kept M_1, M_2 and M_4 heavy enough such that they decouple from the rest of the spectra.

III. CONSTRAINTS

The LHC collaborations have explored various signal regions for any possible hint of a Z'. The most stringent

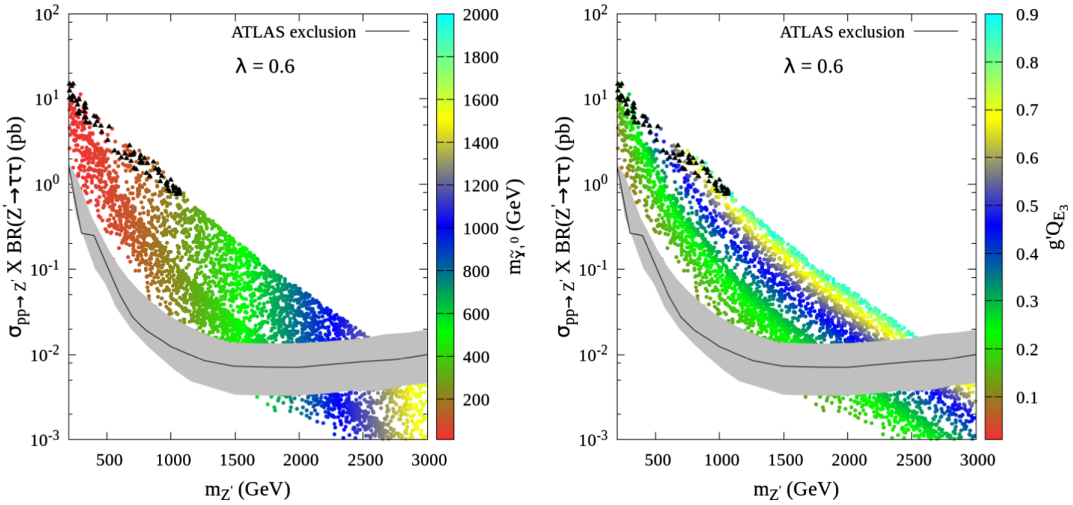

FIG. 1. Impact of the existing exclusion limit on $m_{Z'}$ from the $Z' \to \tau\tau$ search channel with $\lambda = 0.6$. The color coding represents the variation of the LSP neutralino mass or $g' Q_{E_3}$ as indicated in the respective plots. The black points indicate those points that are ruled out from direct chargino-neutralino searches. The gray shaded region represents the 95% exclusion region around the observed limit.

constraint is derived from high-mass dilepton resonance searches which exclude a Z' mass ($m_{Z'}$) up to 4.5 TeV from data accumulated at $\sqrt{s} = 13$ TeV with 139 fb^{-1} luminosity [42]. A search for heavy particles decaying into a top-quark pair results in an exclusion limit on $m_{Z'}$ ranging from 3.1 to 3.6 TeV at $\sqrt{s} = 13$ TeV with 36.1 fb^{-1} luminosity [43]. The dijet resonance search limit on $m_{Z'}$ is slightly weaker, $m_{Z'} > 2.7$ TeV at $\sqrt{s} = 13$ TeV with 36 fb^{-1} luminosity [44]. Thus it is evident that the most stringent constraint on $m_{Z'}$ is derived from its leptonic decay modes. Consequently, models with a leptophobic Z' [37,45–47] are much less constrained in comparison. $Z' \to \tau\tau$ decay deserves a special mention in this regard since the τ can decay both leptonically and hadronically. A combined search of both leptonically and hadronically decaying τ-pairs excludes $m_{Z'}$ up to 2.42 TeV at $\sqrt{s} =$ 13 TeV with 36 fb^{-1} luminosity [48].

These existing exclusion limits are expected to vary depending on the assignments of $U(1)'$ charges (Q) since these affect the production cross section of Z'. In the present scenario, Z' is forbidden to decay into light lepton pairs at the tree level. The Z' therefore, mostly decays via a pair of τ-leptons. This, along with the decay into a neutralino-chargino pair, accounts for most of the Z' width. Thus apart from the direct search limit on $m_{Z'}$, an indirect limit can also be derived from chargino/neutralino search results. This *new* decay mode of the Z' can contribute to the multilepton signal rate at the LHC. A Z' search in such signal regions has not been performed.

Indirect constraints can be derived on $m_{Z'}$ from dark matter requirements. In this work we will focus on singlino and Higgsino LSP scenarios. A pure singlino LSP can only annihilate efficiently around the Higgs and Z' resonances. However, the Higgs resonance region can be safely ruled out from LHC constraints on $m_{Z'}$. The Z' resonance region depends on the choice of model parameters. It is therefore worth checking if one can obtain a sub-TeV singlino dark matter (DM) in the present framework and still be consistent with the exclusion limits on $m_{Z'}$. The relic density requirement forces a pure Higgsino DM to lie above 1 TeV. LSP Higgsino masses below that yield relic underabundance due to too much coannihilation [49]. Direct search limits on the Higgsino mass under such circumstances are weak, around 200 GeV at $\sqrt{s} = 13$ TeV with 139 fb^{-1} luminosity [50].

In order to understand the relevant parameter space, we have carried out detailed scans of the parameter space. The model was implemented in SARAH-4.14.0 [51–55], modifying an existing model. The model files are attached as auxiliary material [56], which does the analytical calculation and writes the required files for implementing the model in numerical packages Spheno-4.0.2 [57–59] and MicrOMEGAS-4.3.5 [60]. Spheno calculates the masses, mixing matrices and the decay branching ratios of all the particles. MicrOMEGAs is used for the DM computations. We intend to explore both the singlino and Higgsino LSP scenarios and hence we divide our scans into small λ and large λ cases.

The λ parameter multiplied by the singlet VEV generates the effective μ-term in this mode, and therefore drives the Higgsino masses. As seen from the neutralino mass matrix, the λ parameter also impacts the singlino-Higgsino mixing. Therefore, when the λ parameter is larger, one obtains a large parameter space where the LSP is a pure singlino and the Higgsinos are heavier than the Z'. In this case, the Z' decays dominantly into a tau pair and hence this parameter space is more likely to be excluded by the ditau search channel. On the other hand, when the λ parameter is smaller, the LSP can be a singlino-Higgsino admixture or even a pure Higgsino one. Apart from the LSP, there can

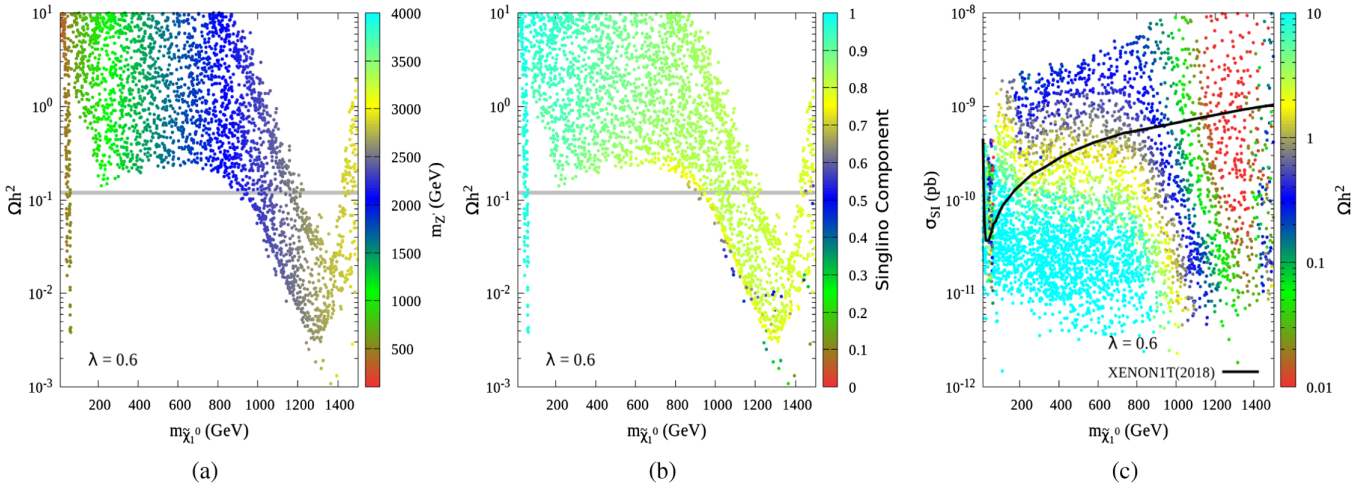

FIG. 2. Distribution of the relic density as a function of the LSP mass with the color gradient representing variation of $m_{Z'}$ (a) and the abundance of the singlino component in the LSP neutralino (b). Plot (c) shows the distribution of the direct detection cross section as a function of LSP mass with the color gradient representing relic density. All the distributions are for $\lambda = 0.6$.

also be additional chargino-neutralino states lying below the Z' and, in the presence of these decay modes, its decay branching ratio into the tau pair is reduced. For this case, the multilepton final state is quite relevant. The benchmark points chosen reflect these facts. We fix all the $U(1)'$ charges by Q_{E_3} and note that these charges always appear together with the coupling g'. We therefore consider $g'Q_{E_3}$ as one single parameter to vary. Below are the parameter ranges that we consider:

$$g'Q_{E_3} \equiv [0.01:0.9]; \quad \tan\beta \equiv [5.0:15.0];$$
$$v_S \equiv [1.0:15.0]\ \text{TeV}, \quad A_\lambda \equiv [1.0:15.0]\ \text{TeV}. \tag{3.1}$$

We have randomly generated points within these parameter ranges. Overall, we have generated about 100,000 points for each scan. Points are then passed through the constraints like 125 GeV Higgs mass, its coupling strengths with standard model particles and flavor constraints. The surviving points are shown in the subsequent figures.

A. Large λ

Throughout this scan we keep $\lambda = 0.6$, $M_1 = M_2 = M_4 = 4$ TeV. All the slepton and squark masses are kept at or above 3 TeV. The exclusion limits, as obtained, are shown in Fig. 1. The color gradient represents either the variation of the LSP neutralino mass or $g'Q_{E_3}$, as indicated in the figure. The exclusion limit obtained from $Z' \to \tau\tau$ search is shown by the black line while the gray shaded area represents the 95% confidence level region around the exclusion line [48]. The black points represent those excluded from direct neutralino-chargino searches [50,61,62]. These constraints do not appear to affect the available parameter region significantly. This is because the λ parameter is relatively large which ensures that the Higgsino mass parameter is quite large compared to the singlino in most of the cases. The bino and wino parameters also being large throughout, both the chargino states and other neutralino states in the spectrum are quite heavy and the singlino is the LSP state, which can still be significantly light. Thus the next to lightest supersymmetric particle (NLSP) pair or the LSP-NLSP associated production cross sections are very small. On the other hand, the LSPs can be produced copiously, but they are completely invisible. As expected, the exclusion limit on $m_{Z'}$ becomes weaker as $g'Q_{E_3}$ is decreased since the production cross section drops with it. As is evident, with $g'Q_{E_3} \sim 0.2$, the exclusion limit can be much weaker, $m_{Z'} \gtrsim 1500$ GeV.

Now let us look at the DM properties. The distribution of the relic density as a function of the LSP neutralino mass is shown in Fig. 2. The color coding in the plots from left to right indicates the variation of $m_{Z'}$, the abundance of the singlino component in the LSP and the relic density respectively. The horizontal shaded band represents the 2σ allowed region around the correct relic abundance, 0.119 ± 0.0054 [63]. The XENON limit [64] on the direct detection cross section (σ_{SI}) is shown by the black curve. The two distinct resonance regions shown in the figure are due to the two CP-even Higgs masses corresponding to the MSSM Higgs doublets. For small $g'Q_{E_3}$ the LSP is dominantly singlino, resulting in very small σ_{SI} which increases as the LSP becomes a singlino-Higgsino admixture. The admixture of singlino and Higgsino produces more underabundance of relic density below 1.4 TeV, yielding a wider range of parameter space satisfying the relic density requirement. Note that the LHC limit on $m_{Z'} \gtrsim 2$ TeV rules out a significant portion of the DM allowed parameter region as indicated by blue points in Fig. 2(a).

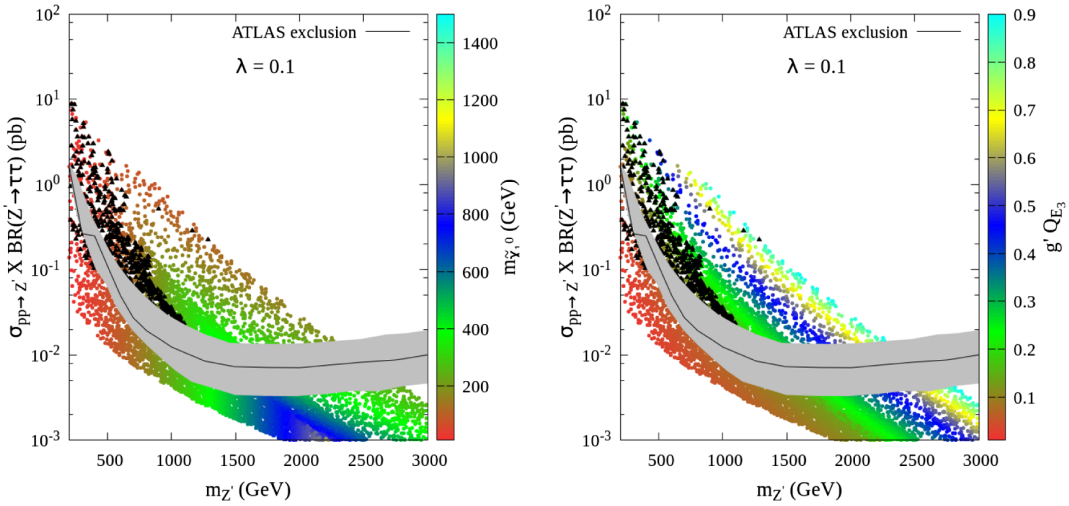

FIG. 3. Impact of the existing exclusion limit on $m_{Z'}$ from the $Z' \to \tau\tau$ search channel with $\lambda = 0.1$. The color coding represents the variation of the LSP neutralino mass or $g' Q_{E_3}$ as indicated in the respective plots. The black points indicate points ruled out from direct chargino-neutralino searches. The gray shaded region represents the 95% exclusion region around the observed limit.

B. Small λ

Throughout this scan we keep $\lambda = 0.1$, $M_1 = M_2 = M_4 = 4$ TeV. All the slepton and squark masses are kept at or above 3 TeV. The exclusion limits, as obtained, are shown in Fig. 3. The color gradient represents either the variation of the LSP neutralino mass or $g' Q_{E_3}$ as indicated in the figure. The exclusion limit is taken from the most recent results published by the ATLAS Collaboration [48]. It is evident that for small enough $g' Q_{E_3}$, even sub-TeV $m_{Z'}$ is allowed from $Z' \to \tau\tau$ searches. However, some of this parameter space may already be excluded from neutralino-chargino search results at the LHC. Since the bino and wino soft mass parameters are decoupled from the rest of the spectrum, the LSP can be either a singlino or Higgsino. Depending on the nature of the LSP, the exclusion limits on the LSP-NLSP masses can be distinctly different. The black points in Fig. 3 represent these excluded regions. The region below the Z' exclusion limit remains unaffected from the neutralino-chargino searches. The region with $m_{Z'} \lesssim 500$ GeV merits a closer look since some of the neutralino-chargino masses are expected to be light enough to be produced in abundance at the LHC. It turns out that all the allowed points shown in the figure have a very small LSP-NLSP mass gap and hence may avoid detection. We checked some sample points from these regions through CheckMATE-2.0.24 [65,66] that they are indeed allowed from the latest neutralino-chargino search results' constraints [50,61,62].

The distribution of relic density and direct detection cross section of the LSP in this scenario are shown in Fig. 4.

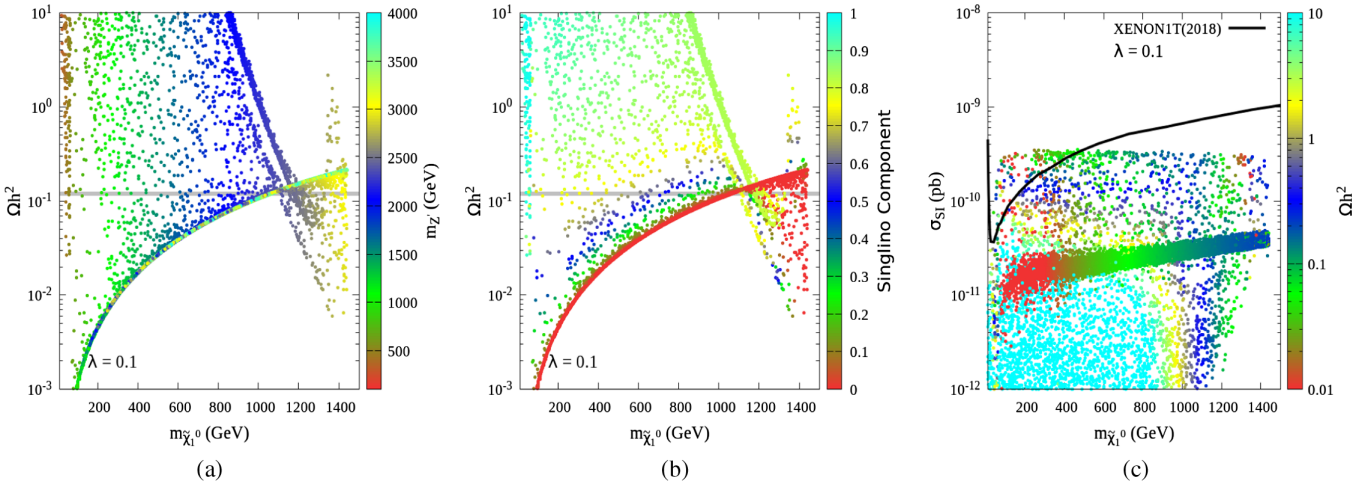

FIG. 4. Distribution of the relic density as a function of the LSP mass with the color gradient representing the variation of $m_{Z'}$ (a) and the abundance of the singlino component in the LSP neutralino (b). Panel (c) shows the distribution of direct detection cross section as a function of LSP mass with the color gradient representing relic density. All the distributions are for $\lambda = 0.1$.

The λ parameter being smaller, one would expect the effective μ-term to be smaller in comparison with the previous case. Hence there is a large region of parameter space where the LSP is purely Higgsino-like or a well-mixed singlino-Higgsino state. The abundance of the red points in Fig. 4(b) illustrates this feature. As expected, for sub-TeV neutralino states, these points result in an underabundance of relic density due to too much coannihilation. However, there is also a significant amount of parameter space where the points produce just the correct relic abundance with well-mixed singlino-Higgsino LSP states, as represented by the blue and green points. These points are also safe from Z' searches with $m_{Z'} \gtrsim 1.5$ TeV as can be observed from Fig. 4(a). The direct-detection constraint is not too severe in this case. For the pure Higgsino LSP [indicated by the red points in Fig. 4(b)], the contributions from two Higgsino components cancel each other. A singlino-Higgsino admixture produces larger σ_{SI}, but beyond $m_{\chi_1^0} > 500$ GeV, the parameter space is safe from the XENON limit.

In the next section we present some representative benchmark points with the input parameters and resulting mass spectra and decay branching ratios. For large λ we observed that only the singlino LSP state lies below $m_{Z'}$ and therefore, the SUSY decay mode of the Z' is completely invisible. For smaller λ, as g' increases, there is more mixing between the singlino and Higgsino states and as a result additional neutralino-chargino states start to appear in between the Z' and the LSP. Now Z' may decay into $\tilde{\chi}_i^0\tilde{\chi}_j^0$ or $\tilde{\chi}_1^{\pm}\tilde{\chi}_1^{\mp}$ states that eventually yield dilepton or trilepton final states. In principle, a four-lepton final state is also possible when a pair of heavier neutralinos produced from Z' decay via the $\ell\bar{\ell}\tilde{\chi}_1^0$ mode.

C. Benchmark points

From the discussion above, the relevant parameter region can be represented by three different classes of benchmark points.

(i) *Class I*: The masses are aligned in such a way that the Z' can decay into both the Higgsino and singlino type neutralino-chargino states. Thus there are three neutralinos and one chargino lying below $m_{Z'}$ and there is a sizable mass gap between LSP singlino and NLSP Higgsino states, such that the resulting decay leptons can be hard enough. This class of points is shown in Fig. 3.

(ii) *Class II*: The hierarchy of masses is similar to that in class I, except for the fact that the LSP can be singlino or Higgsino dominated or a well-mixed state. The NLSP-LSP mass gap is small and thus the final state leptons are softer. This class of points is also shown in Fig. 3.

(iii) *Class III*: Only the LSP state is lighter than the Z'. The LSP can either be a singlino or Higgsino. The NLSP has a mass that kinematically forbids Z' to decay into any chargino or neutralino pairs. Otherwise, it is simply heavier than Z'. In this case, the Z' has a large invisible branching ratio. This class of points is shown in Fig. 1.

In the next section, we shall concentrate only on benchmark points belonging to class I and class II since the Z' in Benchmark Point (BP5) has no visible decay into SUSY particles.

IV. COLLIDER ANALYSIS

So far, we observed that for small enough values of Q_{E_3}, the Z' can easily avoid detection in the conventional search channels at the LHC. Under such circumstances, although the Z' has a significantly large decay branching ratio into the $\tau\tau$ mode, the production cross section is simply not large enough for Z' to be detected. Within a SUSY framework, however, the Z' has additional decay modes that can be explored. Lowering the Q_{E_3}, g' and v_S parameters results in small Z' masses. At the same time these also lower the singlino mass. Additionally, for small λ choices, there can be Higgsino-like neutralino and chargino states lying below the $m_{Z'}$. Hence the Z' can easily decay into $\tilde{\chi}_i^{\pm}\tilde{\chi}_j^{\mp}$ and $\tilde{\chi}_i^0\tilde{\chi}_j^0$ modes. Note that in principle, the bino and wino dominated states can also easily have masses lying in between Z' and the LSP. This can result in a rich cascade decay starting from the resonance production of Z', but the constraints on bino- and wino-like neutralino-chargino states are comparatively more severe[4] [50,67,68]. The Higgsino LSP scenario is understandably the least constrained one since its production cross section is comparatively smaller and the NLSP-LSP states are mass degenerate. Note however that the constraints on binos and winos are not that robust, so looking at light binos and winos in this model might prove an interesting avenue to pursue in future work.

Depending on the number of neutralino-chargino states lying below $m_{Z'}$, the observable final states can be quite different. A large parameter space discussed so far has either the singlino- or the Higgsino-dominated states accessible to the Z' decays. In that case, the Z' decays invisibly into these channels and the $\tau\tau$ decay mode is the one more likely to be seen first. If both the singlino and the Higgsino states lie below $m_{Z'}$, from the cascade decay one can expect to obtain two or more leptons in the final state associated with missing energy. Therefore, we use the multilepton search results from the LHC to ascertain the sensitivity of this search strategy for probing Z' in the present scenario. We then proceed to make an estimate of the LHC sensitivity at high luminosity. Note that the sensitivity of these multilepton search strategies in probing the present scenario is likely to

[4]In that case, quite a large portion of the parameter region with sub-TeV $m_{Z'}$ will be discarded based on the bino-wino search results. Thus it is safe to assume that the bino and wino mass parameters are much heavier than $m_{Z'}$.

TABLE II. Relevant masses and branching ratios of the benchmark points studied here. Here $i(j) \equiv 2, 3$ and $k \equiv 1, 2, 3$.

Parameters and branching ratio (BR)	Class I		Class II		Class III
	BP1	BP2	BP3	BP4	BP5
$\tan\beta$	10.0	11.6	14.36	10.12	7.25
Q_{E_3}	0.5	0.5	0.65	0.65	0.91
g'	0.3	0.3	0.3	0.3	0.3
λ	0.1	0.1	0.1	0.1	0.6
v_S (GeV)	9203.0	10562.0	8590.3	8840.0	8745.9
m_{h_1} (GeV)	124.8	124.7	125.7	125.0	126.2
m_{h_2} (GeV)	1381.1	1584.9	1670.0	1734.8	2741.2
$m_{Z'}$ (GeV)	1379.7	1572.8	1670.6	1735.6	2400.2
$m_{\tilde{\chi}_1^0}$ (GeV)	428.5	543.1	600.1	633.0	1075.0
$m_{\tilde{\chi}_2^0}$ (GeV)	666.3	764.3	622.9	640.1	3713.4
$m_{\tilde{\chi}_3^0}$ (GeV)	668.7	766.7	630.0	656.4	3732.9
$m_{\tilde{\chi}_1^\pm}$ (GeV)	667.4	765.4	624.0	641.1	3717.9
BR($Z' \to \tau\bar{\tau}$)	0.45	0.48	0.35	0.35	0.65
BR($Z' \to \tilde{\chi}_1^0\tilde{\chi}_1^0$)	0.18	0.14	0.05	⋯	0.06
BR($Z' \to \tilde{\chi}_i^0\tilde{\chi}_j^0$)	0.09	0.09	0.24	0.29	⋯
BR($Z' \to \tilde{\chi}_1^\pm\tilde{\chi}_1^\mp$)	0.09	0.08	0.20	0.20	⋯
BR($Z' \to q_k\bar{q}_k$)	0.19	0.21	0.16	0.16	0.29

vary depending on the mass difference between the light neutralino-chargino states [50,67,68]. Two sets of kinematic cuts are therefore chosen in such a way so as to gain maximum possible sensitivity for the different sets of benchmark points.

For our collider analysis, we have used MadGraph5 [69,70] to generate events at the parton level which are subsequently passed through PYTHIA8 [71,72] for decay, showering and hadronization. The nn23lo1 parton distribution function [73,74] has been used while simulating signal as well as SM background events. The MLM matching [75,76] scheme has been used for production channels with light jets at the parton level. We have used the anti-kt algorithm [77] in FastJet [78] for construction of jets and Delphes [79–81] for detector simulation. Finally, we perform our analysis in CheckMATE [65,66].

A. Cuts for benchmark points class I

For this class of benchmark points, apart from ditaus, dileptons associated with missing transverse energy can be a possible signal. Note that contribution to this new signal region for Z' can only arise from the small branching ratio of its decay into the charginos or neutralino states. As can be observed from Table II, a Z' branching ratio of 18% for the decay is relevant to this case, which is further diminished by the leptonic branching ratio of the decay of the gauge bosons. Hence the resultant event rate is expected to be small and the ditau signal region is expected to be observed first if such a Z' exists. However, the dileptonic signal region, if observed further at high luminosity, can serve as a robust hint of the existence of SUSY.

TABLE III. Cut-flow table for signal and SM background channels for BP1 and BP2 benchmarks.

Channels	Cross section (fb)					
	C1	C2	C3	C4	C5	C6
BP1	1.008	0.572	0.544	0.504	0.207	0.007
BP2	0.593	0.330	0.313	0.291	0.133	0.005
$t\bar{t}$ + jets	13823.5	7756.9	423.1	406.6	6.535	⋯
$t\bar{t} + X$	85.992	37.568	0.546	0.497	0.032	⋯
VV	1755.233	1362.872	1343.398	1086.805	1.104	0.003
VVV	15.021	4.119	2.966	2.430	0.117	0.012

The dominant SM background channels for this signal region are $t\bar{t}$ + jets; $t\bar{t} + V$ $(V = W^\pm, Z)$; $t\bar{t} + h$; VV; VVV; and Z + jets. We set the following criteria for selection of the final state.

(i) *C1*: The final state must have two opposite-sign different flavor leptons. The transverse momenta p_T of the leading and subleading leptons are required to be more than 25 and 20 GeV respectively.
(ii) *C2*: No central light jets with $p_T > 40$ GeV and $|\eta| < 2.4$.
(iii) *C3*: No central b-tagged jets with $p_T > 20$ GeV and $|\eta| < 2.4$.
(iv) *C4*: The invariant mass of the opposite-sign dilepton pair $m_{\ell\ell}$ has to be away from the Z-boson mass (m_Z), i.e., $|m_{\ell\ell} - m_Z| > 10$ GeV.
(v) *C5*: The missing transverse energy $\not{E}_T$ has to be more than 200 GeV.
(vi) *C6*: The transverse mass, m_{T_2}=$\min_{\vec{q}_T}[\max(m_T(\vec{p}_T^{\ell_1}, \vec{q}_T), m_T(\vec{p}_T^{\ell_2}, \vec{p}_T^{\text{miss}} - \vec{q}_T))]$, should be more than 150 GeV. Here m_T is given by $m_T(\vec{p}_T, \vec{q}_T) = \sqrt{2(p_T q_T - \vec{p}_T.\vec{q}_T)}$.

B. Results for benchmark points class I

The resulting cross-sections after each cuts (C1–C6) for benchmark points BP1 and BP2 along with the relevant background channels are shown in Table III. In this case the gauge boson production channels are the most dominating contributors to the background. Cuts C5 and C6 effectively reduce these contributions. Cuts C2 and C3 are particularly helpful in reducing the backgrounds from top production channels which are further reduced by C6. The requirement that the leptons need to be different flavors is helpful in reducing the leptons arising from the Z boson decay. Including the same-flavor lepton pairs enhances the signal rate, but the background contribution especially from the VV production channel becomes too large even in the

TABLE IV. Cut-flow table for signal and SM background channels for BP3 and BP4 benchmarks.

	Cross section (fb)					
Channels	D1	D2	D3	D4	D5	D6
BP3	0.168	0.083	0.072	0.010	0.003	0.003
BP4	0.025	0.013	0.011	0.004	0.002	0.002
$t\bar{t}+\text{jets}$	2749.1	2670.6	709.87	4.392	0.088	0.003
$t\bar{t}+X$	11.56	11.48	2.208	0.047	0.002	⋯
VV	339.51	73.52	67.14	0.753	0.305	0.005
VVV	1.193	0.937	0.737	0.017	0.006	0.001

presence of cut C4. The large m_{T_2} cut proves to be most effective in getting rid of the background although it also reduces the signal events to a large extent. Overall, one requires an integrated luminosity of ∼1.4 and ∼2.6 ab^{-1} to exclude (or to achieve 2σ statistical significance) BP1 and BP2 respectively.[5] To achieve a 3σ statistical significance one requires ∼3.1 and ∼6 ab^{-1} integrated luminosity respectively. The high-luminosity LHC is expected to reach an integrated luminosity of 3 ab^{-1}. There is also one high-energy LHC proposal that will operate at 27 TeV and is expected to reach 15 ab^{-1} luminosity.

C. Cuts for benchmark points class II

Benchmark points under class II have a smaller NLSP-LSP mass gap and as a result we cannot use a hard m_{T_2} cut to reduce background contributions effectively. Instead, we devised the cuts in such a way so that the softness of the leptons and the large missing energy can be utilized to reduce the SM events. The criteria used here are as follows:

(i) *D1*: The final state must have two opposite-sign leptons with their p_T within the range [5, 30] GeV. For electrons, $|\eta_e| < 2.4$ and for muons, $|\eta_\mu| < 2.5$.
(ii) *D2*: At least one light jet with $p_T > 25$ GeV and $|\eta| < 2.4$.
(iii) *D3*: No central b-tagged jets with $p_T > 25$ GeV and $|\eta| < 2.4$.
(iv) *D4*: Missing energy, $\not{E}_T > 250$ GeV.
(v) *D5*: Transverse mass, $m_T(\ell_i, \not{E}_T) < 70$ GeV, where $i = 1, 2$.
(vi) *D6*: Invariant mass of opposite-sign lepton pair, $4 < m_{\ell\ell} < 25$ GeV.

The resulting cross-sections after each cuts (D1–D6) for benchmark points BP3 and BP4 along with the relevant background channels are shown in Table IV. In order to reduce the background contributions from the gauge boson production channels, we put strict restrictions on the transverse mass of the charged leptons and missing energy. This cut, combined with the large missing energy one, effectively reduces the background contributions. A further restriction on the invariant mass of the same-flavor lepton pairs ensures that even such a small signal rate can be observed at the high-luminosity LHC. Reducing the VV background proves to be difficult in this case. Demanding the presence of at least one hard jet coupled with a large missing energy cut is useful to this effect. Moreover, demanding a small invariant mass window (D6) reduces this background effectively. The resulting statistical significance of this class of benchmark points is understandably small due to the smaller production cross section of the signal. BP3 and BP4 require an integrated luminosity of ∼4 and ∼10 ab^{-1} respectively to achieve a 2σ statistical significance. To obtain 3σ, one requires ∼10 and ∼22 ab^{-1} respectively.

Note that the large luminosity requirement for BP4 observation makes it most unlikely to be probed at the LHC in the above-mentioned signal region mainly because of the very small NLSP-LSP mass gap (∼7 GeV). For these kind of points, one can consider probing a monojet signal region where one of the initial-state-radiation (ISR) jets is tagged [50]. However, this signal region has large a hadronic background that is almost impossible to get rid of against such a small signal rate.

V. CONCLUSION

We have considered a scenario where the MSSM is extended by one additional $U(1)'$ gauge group. The $U(1)'$ charges for the fermions and Higgs bosons are family dependent, which allows for cancellation of anomalies without the introduction of exotic states, and leads to interesting phenomenological consequences. We consider one possible solution to all the anomaly cancellation conditions in such a way that all the $U(1)'$ charges can be written in terms of Q_{E_3}, the corresponding $U(1)'$ charge for E_3^c. The resulting charge assignments require one to introduce a nonholomorphic SUSY breaking Lagrangian to the theory in order to avoid massless fermions. They also forbid the Z' decay into an electron or muon pair at the tree level, which circumvents the most stringent constraint on $m_{Z'}$. In the absence of these decay modes the restriction on $m_{Z'}$ arises from Z' decay into the $\tau\bar{\tau}$ final state, which is understandably much weaker. The signal cross section is also dependent on the choice of $U(1)'$ charges and other possible decay modes of Z'. In the framework of SUSY, there can be some other decay modes. Here we have explored the possibility of its decay into multiple chargino and neutralino states that can give rise to observable leptonic signals at a high-luminosity LHC. Since we are working within a R-parity conserving framework, the LSP neutralino can be a DM candidate. A nonstandard candidate for LSP such as a singlino or a Higgsino arises naturally in this framework if one considers a light Z'. Hence we restricted ourselves to these two possibilities and performed

[5]To compute statistical significance we have used $\mathcal{S} = \sqrt{2(S+B)\text{Log}(1+\frac{S}{B}) - S}$.

a scan of the parameter space by varying λ, $\tan\beta$, and $g'Q'$, where $Q' \equiv Q'_{E_3}$ to highlight the available parameter space taking into account both the collider and DM constraints. We proceed to study two possible signal regions with a pair of opposite-sign leptons in the final state with different sets of kinematic cuts chosen suitably depending on the varying NLSP-LSP mass gap. We observed that even in the presence of these additional decay modes, the ditau final state is likely to be observed first and if it so happens, one can use the leptonic signal regions as confirmatory channels. In the present framework, any observation of such leptonic signals at high luminosity will also indicate the presence of SUSY.

ACKNOWLEDGMENTS

M. F. acknowledges Natural Sciences and Engineering Research Council of Canada (NSERC) for partial financial support under Grant No. SAP105354. S. M. and K. H. acknowledge H2020-MSCA-RISE-2014 Grant No. 645722 (NonMinimal Higgs).

[1] N. Okada and O. Seto, Phys. Rev. D **82**, 023507 (2010).
[2] N. Okada and S. Okada, Phys. Rev. D **95**, 035025 (2017).
[3] N. Okada and S. Okada, Phys. Rev. D **93**, 075003 (2016).
[4] P. Agrawal, N. Kitajima, M. Reece, T. Sekiguchi, and F. Takahashi, arXiv:1810.07188.
[5] J. Heeck and W. Rodejohann, Phys. Rev. D **84**, 075007 (2011).
[6] B. Allanach, F. S. Queiroz, A. Strumia, and S. Sun, Phys. Rev. D **93**, 055045 (2016); **95**, 119902(E) (2017).
[7] M.-C. Chen, J. Huang, and W. Shepherd, J. High Energy Phys. 11 (2012) 059.
[8] P. Fayet, Phys. Lett. **69B**, 489 (1977).
[9] Yu. Ya. Komachenko and M. Yu. Khlopov, Yad. Fiz. **51**, 1081 (1990) [Sov. J. Nucl. Phys. **51**, 692 (1990)].
[10] M. Cvetic and P. Langacker, Mod. Phys. Lett. A **11**, 1247 (1996).
[11] D. Suematsu and Y. Yamagishi, Int. J. Mod. Phys. A **10**, 4521 (1995).
[12] V. Jain and R. Shrock, arXiv:hep-ph/9507238.
[13] Y. Nir, Phys. Lett. B **354**, 107 (1995).
[14] E. Keith and E. Ma, Phys. Rev. D **54**, 3587 (1996).
[15] C. D. Carone, L. J. Hall, and H. Murayama, Phys. Rev. D **54**, 2328 (1996).
[16] C. D. Froggatt and H. B. Nielsen, Nucl. Phys. **B147**, 277 (1979).
[17] J. L. Hewett and T. G. Rizzo, Phys. Rep. **183**, 193 (1989).
[18] M. Cvetic and P. Langacker, Phys. Rev. D **54**, 3570 (1996).
[19] C. T. Hill and E. H. Simmons, Phys. Rep. **381**, 235 (2003); **390**, 553(E) (2004).
[20] D. E. Kaplan and G. D. Kribs, Phys. Rev. D **61**, 075011 (2000).
[21] J. Erler, Nucl. Phys. **B586**, 73 (2000).
[22] S. F. King, S. Moretti, and R. Nevzorov, Phys. Lett. B **650**, 57 (2007).
[23] D. A. Demir, G. L. Kane, and T. T. Wang, Phys. Rev. D **72**, 015012 (2005).
[24] R. Aaij *et al.* (LHCb Collaboration), Phys. Rev. Lett. **113**, 151601 (2014).
[25] R. Aaij *et al.* (LHCb Collaboration), J. High Energy Phys. 08 (2017) 055.
[26] G. Hiller and F. Kruger, Phys. Rev. D **69**, 074020 (2004).
[27] B. C. Allanach, J. Davighi, and S. Melville, J. High Energy Phys. 02 (2019) 082.
[28] A. Celis, J. Fuentes-Martin, M. Jung, and H. Serodio, Phys. Rev. D **92**, 015007 (2015).
[29] B. C. Allanach, J. M. Butterworth, and T. Corbett, J. High Energy Phys. 08 (2019) 106.
[30] J. S. Alvarado, C. E. Diaz, and R. Martinez, Phys. Rev. D **100**, 055037 (2019).
[31] S. F. Mantilla, R. Martinez, and F. Ochoa, Phys. Rev. D **95**, 095037 (2017).
[32] Y. Tang and Y.-L. Wu, Chin. Phys. C **42**, 033104 (2018).
[33] J. F. Kamenik, Y. Soreq, and J. Zupan, Phys. Rev. D **97**, 035002 (2018).
[34] B. Coleppa, S. Kumar, and A. Sarkar, Phys. Rev. D **98**, 095009 (2018).
[35] M. Aaboud *et al.* (ATLAS Collaboration), Phys. Rev. D **96**, 052004 (2017).
[36] Search for a high-mass resonance decaying into a dilepton final state in 13 fb^{-1} of pp collisions at $\sqrt{s} = 13$ TeV, CERN Technical Report No. CMS-PAS-EXO-16-031, 2016.
[37] J. Y. Araz, G. Corcella, M. Frank, and B. Fuks, J. High Energy Phys. 02 (2018) 092.
[38] J. Y. Araz, M. Frank, and B. Fuks, Phys. Rev. D **96**, 015017 (2017).
[39] M. Frank and S. Mondal, Phys. Rev. D **90**, 075013 (2014).
[40] Y. Hiylmaz, M. Ceylan, A. Altas, L. Solmaz, and C. S. Un, Phys. Rev. D **94**, 095001 (2016).
[41] L. Darm, K. Kowalska, L. Roszkowski, and E. M. Sessolo, J. High Energy Phys. 10 (2018) 052.
[42] G. Aad *et al.* (ATLAS Collaboration), Phys. Lett. B **796**, 68 (2019).
[43] M. Aaboud *et al.* (ATLAS Collaboration), Phys. Rev. D **99**, 092004 (2019).
[44] A. M. Sirunyan *et al.* (CMS Collaboration), J. High Energy Phys. 08 (2018) 130.
[45] K. S. Babu, C. F. Kolda, and J. March-Russell, Phys. Rev. D **54**, 4635 (1996).
[46] D. Suematsu, Phys. Rev. D **59**, 055017 (1999).
[47] C.-W. Chiang, T. Nomura, and K. Yagyu, J. High Energy Phys. 05 (2014) 106.

[48] M. Aaboud *et al.* (ATLAS Collaboration), J. High Energy Phys. 01 (2018) 055.
[49] K. Kowalska and E. M. Sessolo, Adv. High Energy Phys. **2018**, 6828560 (2018).
[50] M. Aaboud *et al.* (ATLAS Collaboration), Phys. Rev. D **97**, 052010 (2018).
[51] F. Staub, arXiv:0806.0538.
[52] F. Staub, Comput. Phys. Commun. **181**, 1077 (2010).
[53] F. Staub, Comput. Phys. Commun. **182**, 808 (2011).
[54] F. Staub, Comput. Phys. Commun. **185**, 1773 (2014).
[55] F. Staub, Adv. High Energy Phys. **2015**, 840780 (2015).
[56] See Supplemental Material at http://link.aps.org/supplemental/10.1103/PhysRevD.100.115018 for auxiliary material.
[57] W. Porod, Comput. Phys. Commun. **153**, 275 (2003).
[58] W. Porod and F. Staub, Comput. Phys. Commun. **183**, 2458 (2012).
[59] W. Porod, J. High Energy Phys. 05 (2002) 030.
[60] G. Belanger, F. Boudjema, A. Pukhov, and A. Semenov, Comput. Phys. Commun. **185**, 960 (2014).
[61] G. Aad *et al.* (ATLAS Collaboration), J. High Energy Phys. 05 (2014) 071.
[62] M. Aaboud *et al.* (ATLAS Collaboration), Phys. Rev. D **98**, 092012 (2018).
[63] G. Hinshaw *et al.* (WMAP Collaboration), Astrophys. J. Suppl. Ser. **208**, 19 (2013).
[64] E. Aprile *et al.* (XENON Collaboration), Phys. Rev. Lett. **121**, 111302 (2018).
[65] M. Drees, H. Dreiner, D. Schmeier, J. Tattersall, and J. S. Kim, Comput. Phys. Commun. **187**, 227 (2015).
[66] D. Dercks, N. Desai, J. S. Kim, K. Rolbiecki, J. Tattersall, and T. Weber, Comput. Phys. Commun. **221**, 383 (2017).
[67] Search for electroweak production of supersymmetric particles in the two- and three-lepton final state at $\sqrt{s} = 13$ TeV with the ATLAS detector, CERN Technical Report No. ATLAS-CONF-2017-039, 2017.
[68] A. M. Sirunyan *et al.* (CMS Collaboration), Phys. Lett. B **782**, 440 (2018).
[69] J. Alwall, M. Herquet, F. Maltoni, O. Mattelaer, and T. Stelzer, J. High Energy Phys. 06 (2011) 128.
[70] J. Alwall, R. Frederix, S. Frixione, V. Hirschi, F. Maltoni, O. Mattelaer, H. S. Shao, T. Stelzer, P. Torrielli, and M. Zaro, J. High Energy Phys. 07 (2014) 079.
[71] T. Sjostrand, S. Mrenna, and P. Z. Skands, J. High Energy Phys. 05 (2006) 026.
[72] T. Sjostrand, S. Ask, J. R. Christiansen, R. Corke, N. Desai, P. Ilten, S. Mrenna, S. Prestel, C. O. Rasmussen, and P. Z. Skands, Comput. Phys. Commun. **191**, 159 (2015).
[73] R. D. Ball *et al.*, Nucl. Phys. **B867**, 244 (2013).
[74] R. D. Ball *et al.* (NNPDF Collaboration), J. High Energy Phys. 04 (2015) 040.
[75] S. Hoeche, F. Krauss, N. Lavesson, L. Lonnblad, M. Mangano, A. Schalicke, and S. Schumann, in *HERA and the LHC: A Workshop on the Implications of HERA for LHC Physics: Proceedings Part A* (2006).
[76] M. L. Mangano, M. Moretti, F. Piccinini, and M. Treccani, J. High Energy Phys. 01 (2007) 013.
[77] M. Cacciari, G. P. Salam, and G. Soyez, J. High Energy Phys. 04 (2008) 063.
[78] M. Cacciari, G. P. Salam, and G. Soyez, Eur. Phys. J. C **72**, 1896 (2012).
[79] J. de Favereau, C. Delaere, P. Demin, A. Giammanco, V. Lematre, A. Mertens, and M. Selvaggi (DELPHES 3 Collaboration), J. High Energy Phys. 02 (2014) 057.
[80] M. Selvaggi, J. Phys. Conf. Ser. **523**, 012033 (2014).
[81] A. Mertens, J. Phys. Conf. Ser. **608**, 012045 (2015).